A novel histidine functionalized chitosan nanoformulation: Synthesis, characterization and its bioactivity in tomato plant

Mahendra Meena

mahendra966795@gmail.com

SKN Agriculture University

Vinod Saharan

Maharana Pratap University of Agriculture and Technology

K. K. Meena

SKN Agriculture University

Balraj Singh

SKN Agriculture University

Shalini Pilania

Maharana Pratap University of Agriculture and Technology

N. K. Gupta

SKN Agriculture University

Ajay Pal

Chaudhary Charan Singh Haryana Agricultural University

O. P. Garhwal

SKN Agriculture University

Y. K. Sharma

SKN Agriculture University

Uadal Singh

SKN Agriculture University

Rajesh Bagri

SKN Agriculture University

M. K. Sharma

SKN Agriculture University

Rachna Sharma

Dr. B. R. Ambedkar National Institute of Technology Jalandhar

B. L. Jakhar

SKN Agriculture University

Piyush Chandel

Maharana Pratap University of Agriculture and Technology
Damyanti Prajapati
Maharana Pratap University of Agriculture and Technology
Kinjal Mondal
Maharana Pratap University of Agriculture and Technology
Mital Mahala
Maharana Pratap University of Agriculture and Technology
D. K. Bairwa
SKN Agriculture University
Madhu Bai Meena
Maharana Pratap University of Agriculture and Technology

Article

Keywords: Chitosan-histidine nanoformulations, chitosan, histidine, cross-linked, tomato

Posted Date: March 21st, 2024

DOI: https://doi.org/10.21203/rs.3.rs-4002182/v1

Additional Declarations: No competing interests reported.

A novel histidine functionalized chitosan nanoformulation: Synthesis, characterization and its bioactivity in tomato plant

Mahendra Meena[1]*, Vinod Saharan[2], K. K. Meena[3], Balraj Singh[1], Shalini Pilania[4], N. K. Gupta[5], Ajay Pal[6], O. P. Garhwal[3], Y. K. Sharma[3], Uadal Singh[3], Rajesh Bagri[7], M. K. Sharma[1], Rachna Sharma[8], B. L. Jakhar[9], Piyush Chandel[4], Damyanti Prajapati[2], Kinjal Mondal[2], Mital Mahala[2], D. K. Bairwa[10], Madhu Bai Meena[11]

[1]Department of Horticulture, SKNCOA, SKNAU, Jobner, Rajasthan 303 329, India; mahendra.horti@sknau.ac.in, vc@sknau.ac.in; mksharma.horti@sknau.ac.in

[2]Department of Molecular Biology and Biotechnology, Rajasthan College of Agriculture, MPUAT, Udaipur, Rajasthan, India; vinodsaharan@gmail.com, damyanti.1993@gmail.com, kinjal.mondel1234@gmail.com, mkmahala7065@gmail.com

[3]Department of Horticulture, Rajasthan Agricultural Research Institute, SKNAU, Jobner, Rajasthan, India; meenakamal30@gmail.com, opgarhwal.horti@sknau.ac.in, yogeshsharma.rari@sknau.ac.in, usingh.horti@sknau.ac.in

[4]Department of Horticulture, Rajasthan College of Agriculture, MPUAT, Udaipur, Rajasthan, India; qcishalini@gmail.com, piyushchandel1999@gmail.com

[5]Department of Plant Physiology, SKNAU, Jobner, Rajasthan, India; nkgupta.pphy@sknau.ac.in

[6]Department of Biochemistry, College of Basic Sciences and Humanities, Chaudhary Charan Singh Haryana Agricultural University, Hisar, Haryana 125 004, India; ajaydrdo@rediffmail.com

[7]Department of Plant Pathology, Rajasthan Agricultural Research Institute, SKNAU, Jobner, Rajasthan, India; rkbagri.ppath.rari@sknau.ac.in

[8]Department of Chemistry, Dr B R Ambedkar NIT, Jalandhar 144 011, India; rachnanitj@gmail.com

[9]Department of Entomology, Rajasthan Agricultural Research Institute, SKNAU, Jobner, Rajasthan, India; bljakhar.ento@sknau.ac.in

[10]Department of Entomology, SKNCOA, SKNAU, Jobner, Rajasthan 303 329, India; dkbairwa.ento@sknau.ac.in

[11]Department of Plant Pathology, Rajasthan College of Agriculture, MPUAT, Udaipur, Rajasthan, India; madhubaimeena@gmail.com

***Corresponding author**

E-mail: mahendra.horti@sknau.ac.in , mahendra966795@gmail.com

Phone: +91-9351470653; Fax: 01425-254022

Abstract:

The use of novel active ingredients for the functional modification of chitosan nanoformulations has attracted global attention. In this study, chitosan has been functionalized via histidine to craft novel chitosan-histidine nanoformulation (C-H NF) via the ionic gelation method. C-H NF exhibited elite physico-biochemical properties, influencing physiological and biochemical dynamics in tomato crops. Elite properties include homogenous-sized nanoparticles, lower PDI, viscosity, higher zeta potential, nanoparticle concentration/ml, conductivity, encapsulation efficiency, and yield. FTIR spectroscopy revealed histidine interaction with C-H NF, while SEM and TEM exposed its porous structure. Application of C-H NF to tomato seedling and potted plants via seed treatment and foliar spray positively impacts growth parameters, antioxidant-defense enzyme activities, reactive oxygen species (ROS) content, and chlorophyll and nitrogen content. We claim that the histidine-functionalized chitosan nanoformulation enhances physico-biochemical properties, highlighting its potential to elevate biochemical and physiological processes of tomato plant.

Keywords: Chitosan-histidine nanoformulations; chitosan; histidine; cross-linked; tomato

Graphical Abstract:

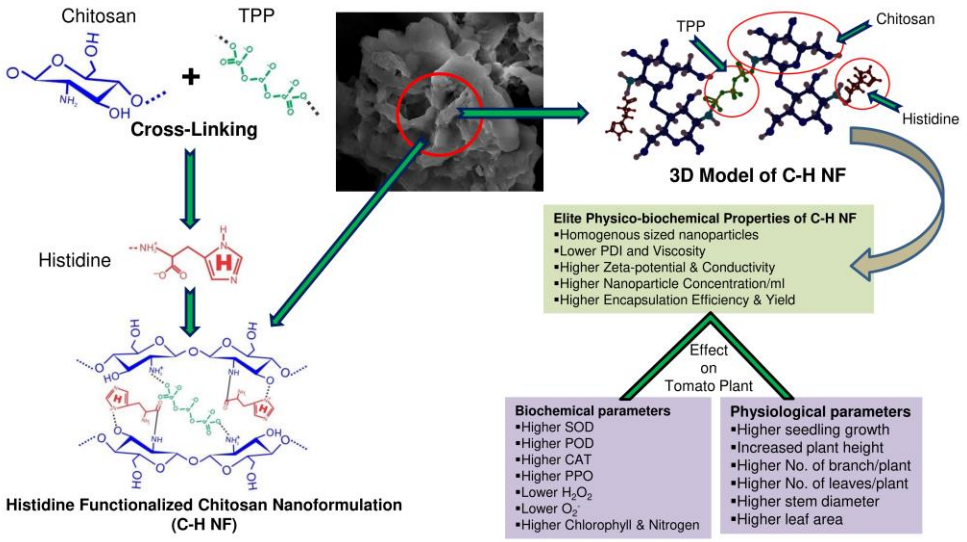

Introduction

Chitosan nanomaterials are highly researched in the agriculture sector by encapsulation of various active ingredients (AIs) *viz.* pesticides, plant hormones, and fertilizers [1, 2]. Encapsulation of AIs helps to amplify the use efficiency of AIs for plant growth and protection. Encapsulations have been done to achieve slow, control, and target delivery and are the main characteristic of chitosan nanomaterials for their application in plant [2]. Further, the immense physico-biochemical activity of the chitosan biopolymer lies in its functional group (C-6 –OH and $–NH_2$). These functional groups provide a broad spectrum platform for enhancing chitosan functionality by attaching AIs [3, 4]. Modification in the functional group significantly alters the size, shape, polydispersity, size distribution, and surface charge of chitosan nanoparticles [5]. Further, modification changes of these physico-biochemical properties considerably affect the biological activity of nanoparticles in plants. In addition, to enhance the bioactivity of chitosan nanoformulations, many AIs have been explored [2]. Various amino acids have been used as AIs to change the properties of chitosan *viz.* arginine, alanine, lysine, proline, histidine, and glutamic acid to raise chitosan-based formulations for use in medical, pharmaceutical, and agriculture [6]. Among the amino acids, histidine has been the most functionally diverse amino acid which has

an imperative role in plant metabolism as a structural and functional component [7, 8]. Chitosan-based formulations incorporated histidine has been documented through diverse methodologies including hydration, crosslinking, fluorimetric, and phase inversion method [6]. These formulations have demonstrated applicability in various fields, such as metal ion absorption as evidenced by studies conducted [9-12]. Furthermore, the versatility of these formulations extends to drug delivery applications [13]. Additionally, research has explored their utility in gene delivery [14-16]. Moreover, the chitosan-based formulations have shown promise in cancer therapy [17], and in the realm of wound healing [18]. However, the method of ionic gelation in which sodium tripolyphosphate (TPP) has been considered to be the method where the payload potential of chitosan nanoparticles increases many folds [2]. This study focuses on the preparation of novel and highly active histidine functionalized chitosan nanoformulations designed to enhance its functionality through the modulation of physico-biochemical properties of nanoparticles. To the best of our knowledge, there haven't been established formulations of this kind of combination as bioactive material in the agriculture field before. Moreover, this study thoroughly explains the synthesis process and the effect of various concentrations of histidine on the physico-biochemical properties of C-H NF. Further, the synthesized nanoformulation was evaluated in test crop tomato as seed treatment and foliar application to measure its biochemical and physiological impact on tomato plants.

Results

Synthesis of C-H NF

In this study, C-H NF synthesis employed the ionic gelation method by crosslinking of 0.5% chitosan and 0.5% TPP. Various histidine concentrations were explored for interaction with the chitosan + TPP complex. Functional groups of histidine interacted with the complex, resulting in

a compact nanoscale chitosan-histidine nanoformulation (C-H NF). Among concentrations (0.5, 1, 1.5, 2, 2.5, and 3%; w/v), 2% histidine exhibited compatibility based on the DLS study. After freeze-drying, approx 386 mg of C-H NF dry powder was obtained per reaction (210 ml).

Physicochemical characterization of C-H NF

DLS, EE, yield, viscosity, and NTA study

C-H NF was synthesized with varying histidine concentrations (0.5-3%; w/v). At 2% histidine, the nanoparticles exhibited a size of 314.4 nm, PDI of 0.218, zeta potential of 11.2 mV, conductivity of 0.046 mS/cm, viscosity of 1.43 Cps, kcps of 406.5, DCR of 1446.4, encapsulation efficiencies of 53%, and yield percentage of 32.17% (Fig. 1; Fig. 4A-I). Further characterization via NTA study revealed 3.53×10^8 C-H NF nanoparticles per ml with a mean size of 341.6± 0.00 nm at pH 7 in an aqueous solution (Fig. 2).

A

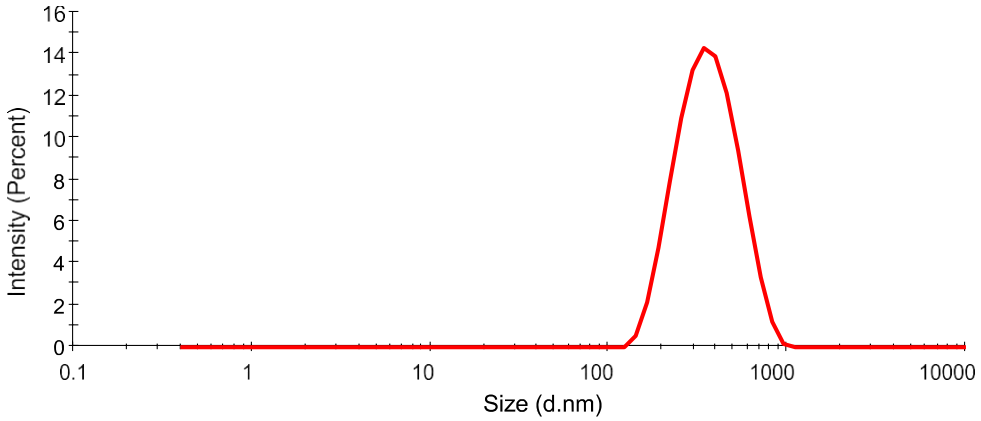
Intensity (Percent)
16
14
12
10
8
6
4
2
0
0.1
1
10
100
1000
10000
Size (d.nm)

B

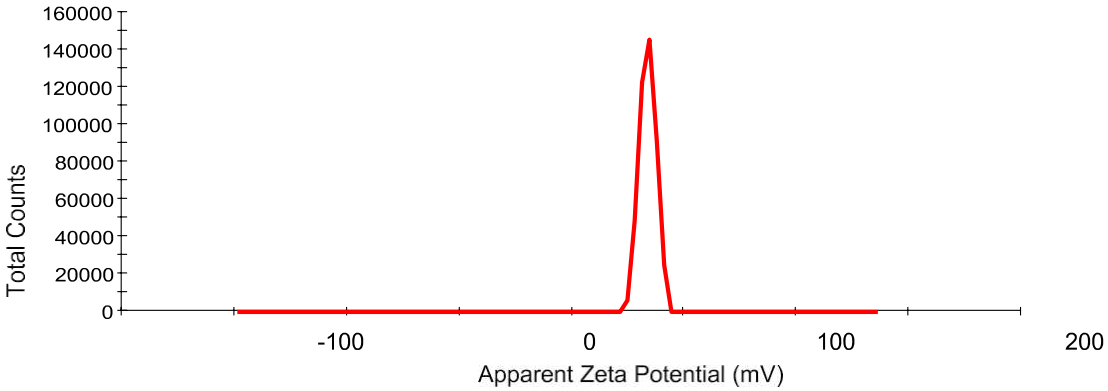
Total Counts
160000
140000
120000
100000
80000
60000
40000
20000
0
-100
0
100
200
Apparent Zeta Potential (mV)

C

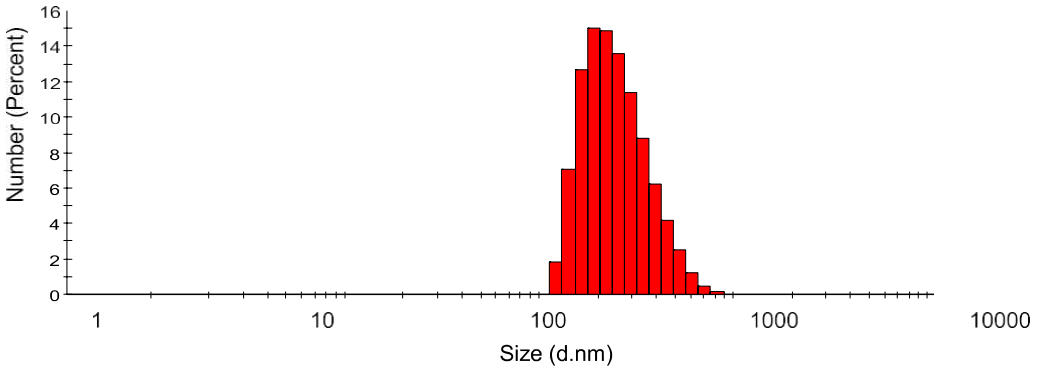

Figure 1. DLS analysis of C-H NF for (A) size (B) zeta potential (C) size distribution by number

A

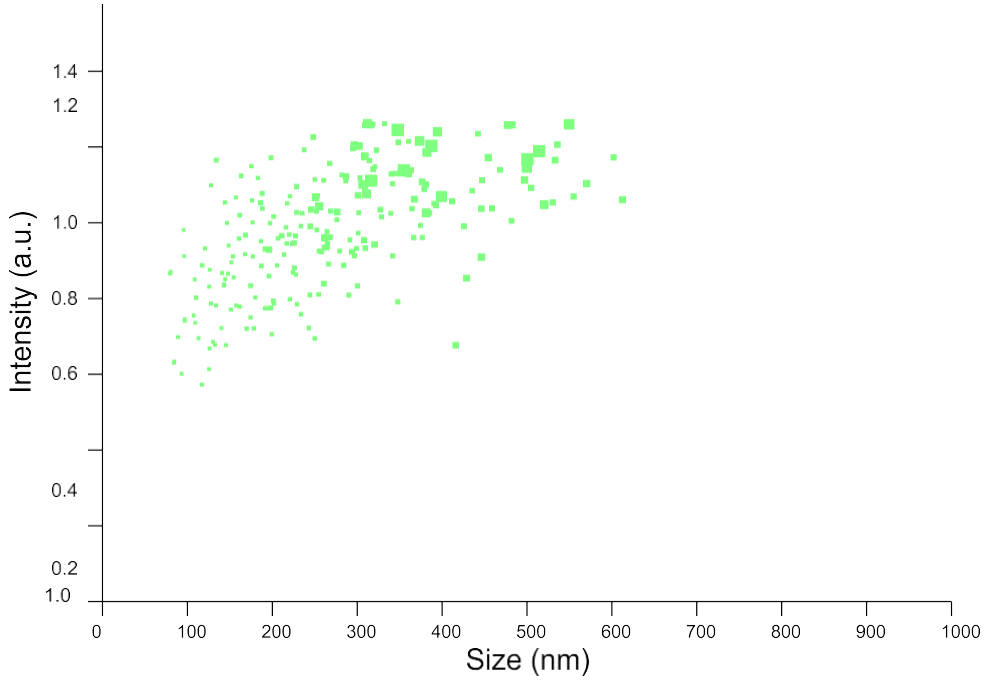

B

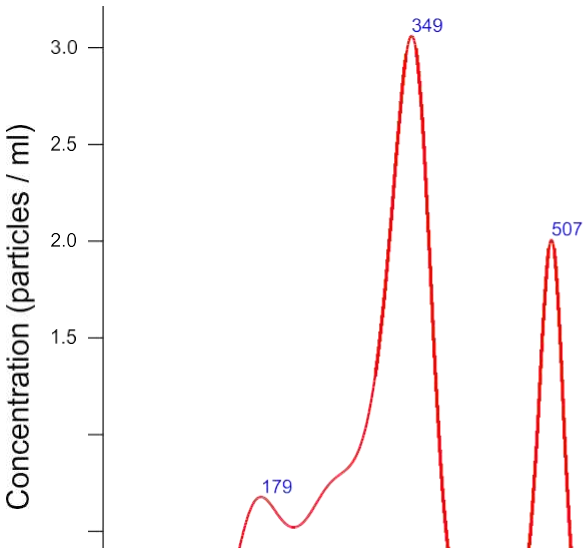

Figure 2: NTA analysis of C-H NF (a) size (b) concentration of particle/ml

FTIR, SEM and TEM of C-H NF

Nanoformulations underwent FTIR analysis for functional group assessment. The main peak at 3439 cm^{-1} in bulk chitosan shifted to 3417 cm^{-1} in C-H NF, indicating alterations in $–NH_2$ and –OH groups (Fig. 3A and B). Peaks shifted 1654 ($–CONH_2$), 1543 ($–NH_2$), and 890 cm^{-1} (anhydrous glycosidic bond) relative to bulk chitosan, revealing chitosan-TPP interaction. A peak at 1648 cm^{-1} in C-H NF corresponding to C=O of histidine interacted with $–NH_2$ of chitosan. Peaks at 2879 cm^{-1} intensified in C-H NF, suggesting the amidation of chitosan. The possibility of histidine's imidazole ring interacting through the –CN to –OH group of chitosan was indicated by the peak shift from 3439 to 3417 cm^{-1}. Further, SEM and TEM studies confirmed the surface morphology and internal structure of C-H NF. SEM (EVO MA10, Carl Zeiss Promenade, Jena, Germany) revealed a spherical nanomaterial with a porous structure (Fig. 3E). However, HR-TEM (HR-TEM, JEOL, JEM 2100F, USA) showed mild pore throughout the structure (Fig. 3F and G).

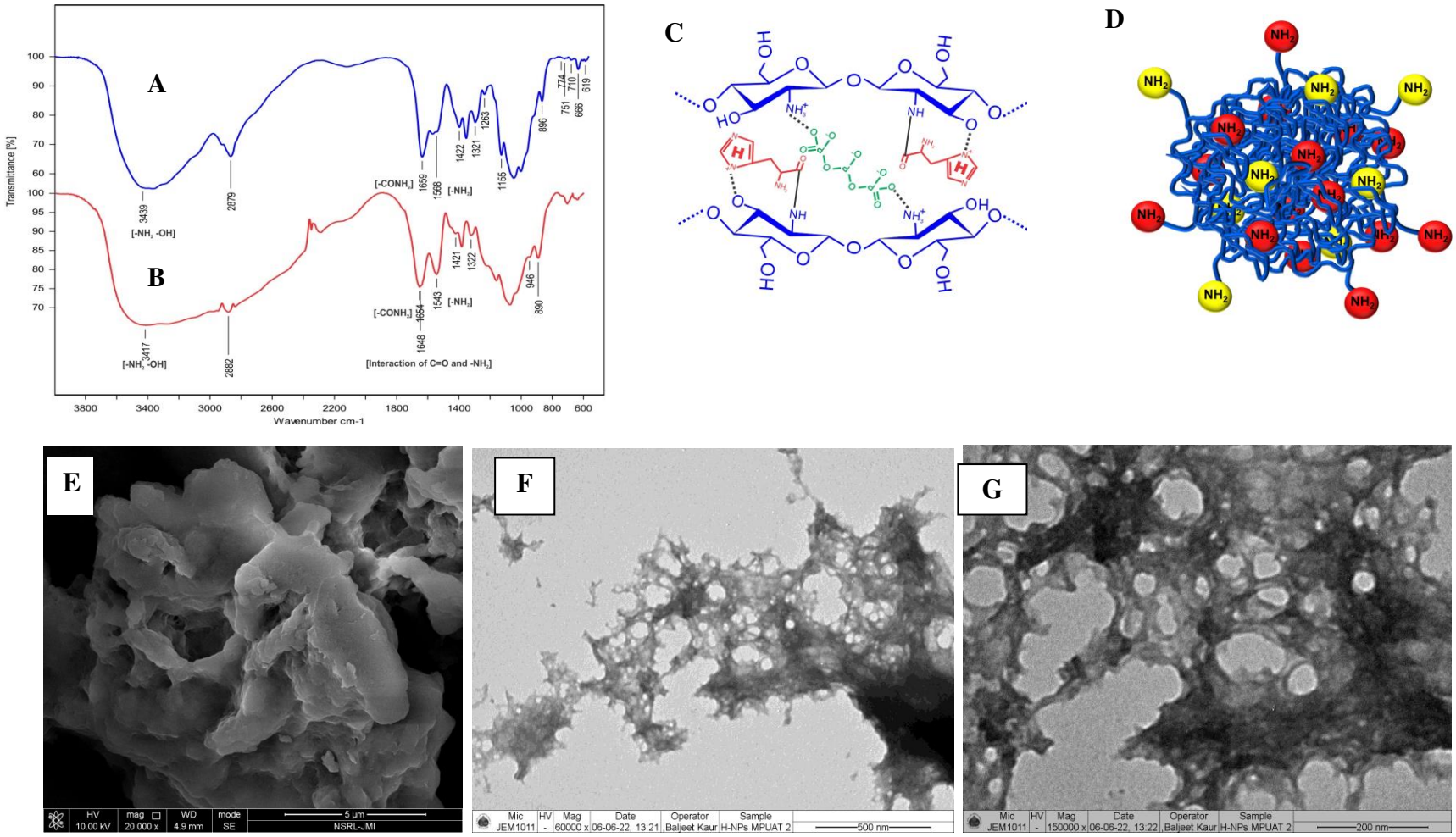

Figure 3: FTIR spectra of (A) bulk chitsan (B) C-H NF (C), (D) hypothetical model of C-H NF showing interactions of chitosan, TPP and histidine and SEM and TEM study of C-H NF, SEM at (E) 20kx, TEM at (F) 60kx (G) 150kx

In-vitro seedling growth

The study investigated the impact of varied C-H NF concentrations (0.001, 0.003, 0.006, 0.012, and 0.015%, w/v) on seedling growth. After a 10-day germination period, results showed a notable positive effect on tomato seedlings, with a significantly higher germination percentage (95.9-99.8%). C-H NF concentrations of 0.006-0.015% demonstrated significant improvements in shoot length (13.6-16.2 cm), root length (10-13.9 cm), and SVI (2556.6-2895.1) compared to histidine (Table 1).

Table 1

Effects of C-H NF on tomato seedling growth in *in-vitro*

Treatments (%)	Seed germination (%)	Shoot length (cm)	Root length (cm)	Seedling vigor index (SVI)
Control (Water)	84.6±0.49^{g}	8.7±0.14^{g}	5.7±0.23^{h}	1221.6±19.6^{i}
BCH (0.01)	91.8±0.57^{f}	10.1±0.05^{f}	7.3±0.16^{g}	1601.5±23.3^{h}
Histidine (0.01)	93.9±0.60^{de}	12.9±0.77^{d}	8.7±0.07^{ef}	2033.0±49.4^{f}
C-H NF				
0.001	91.8±0.49^{f}	11.4±0.49^{e}	8.0±0.03^{f}	1794.8±31.9^{g}
0.003	93.8±0.57^{d}	14.9±0.61^{b}	9.9±0.06^{e}	2367.4±30.8^{d}
0.006	97.9±0.45^{b}	16.2±0.72^{a}	10.0±0.07^{d}	2580.7±42.7^{c}
0.009	99.8±0.66^{a}	15.4±0.49^{ab}	13.8±0.49^{a}	2895.1±67.5^{a}
0.012	99.3±0.61^{a}	13.6±0.60^{c}	13.9±0.49^{a}	2748.1±22.0^{b}
0.015	95.9±0.60^{c}	13.6±0.45^{c}	12.9±0.45^{b}	2556.6±36.6^{c}
0.018	94.9±0.60^{cd}	11.8±0.49^{e}	12.3±0.45^{bc}	2295.2±41.9^{e}

Various growth parameters were recorded at 15 days of tomato seedling. Each value is mean of triplicates and each replicate consisted of 10 seedlings. Error bars represent ±SE (standard error) with the same letter statistically

198 insignificant (p=0.05) as determined by Tukey-Kramer HSD. Water (control) and BCH (bulk chitosan, 0.01%
199 dissolved in 0.1% acetic acid)

200 **Plant growth, antioxidants and defense enzymes, ROS, chlorophyll, and nitrogen content**

201 Growth parameters, including plant height, branch and leaves count per plant, stem diameter,
202 leaf area, and root length were assessed at physiological maturity. In the pot experiment, 0.03-
203 0.15% C-H NF concentration significantly increased plant height (65.3-91.0 cm) compared to
204 control (43.9 cm), BCH (51.0 cm), and histidine (59.2 cm) (Table 2; Fig. 6A). However, the
205 number of branches/plant (11.8-14.9), and leaves/plant (61.1-73.3) with all concentrations
206 exceeded control, BCH, and histidine (Table 2). Additionally, C-H NF (0.01-0.18%) showed
207 effectiveness in stem diameter (7.8-9.4 cm), leaf area (312.8-343.2 cm^2), and root length (30.2-
208 52.7 cm) compared to histidine, BCH and control (Table 2; Fig. 6B). Notably, 0.03-0.15% C-H
209 NF concentration demonstrated effectiveness across all growth parameters in the pot experiment.
210 Following foliar application on pot plants, C-H NF (0.01-0.18% w/v) was examined for
211 antioxidant, defense enzyme activities, ROS, and chlorophyll and N content. In the pot
212 experiment, SOD activity (0.22-0.32 µmol/min/g) significantly surpassed control
213 (0.07µmol/min/g), BCH (0.10µmol/min/g), and histidine (0.19 µmol/min/g) (Table 3). Likewise,
214 POD (0.63-0.86µmol/min/g), CAT (2.6-3.6 mmol/min/g), and PPO (1.6-2.1 µmol/min/g)
215 activities with all C-H NF concentrations were significantly higher than histidine, BCH, and
216 control (Table 3). Conversely, H_2O_2 (176.8-145.3 µmol/g) and O_2^{-1} (54.2-26.2 µmol/g) content in
217 C-H NF (0.01 to 0.18%) was markedly lower than control, BCH, and histidine (Table 3). Total
218 chlorophyll content (2.4-3.3 mg/g) increased notably with all concentrations compared to control
219 (1.56mg/g), BCH (1.94mg/g), and histidine (2.17mg/g) (Table 3). N content (1.62-2.02%) was
220 significantly higher with C-H NF (0.01-0.18%) compared to control (1.40%) (Table 3). Overall,

all C-H NF concentrations exhibited effectiveness in pot plant experiments for antioxidant, defense enzyme activities, ROS, and chlorophyll content.

Table 2

Effect of C-H NF on growth parameters of tomato in pot plant

Treatments (%)	Plant height (cm)	Number of branch/plant	Number of leaves/plant	Stem diameter (mm)	Leaf area (cm^2)	Root length (cm)
Control (Water)	43.9±2.01^{i}	6.9±0.49^{g}	35.9±0.92^{f}	6.0±0.17^{c}	293.2±1.42^{g}	14.1±0.87^{i}
BCH (0.01)	51.0±1.55^{h}	8.9±0.60^{f}	47.6±1.61^{e}	6.4±0.21^{c}	300.4±1.09^{f}	27.6±0.67^{h}
Histidine (0.01)	59.2±0.66^{f}	9.9±0.16^{e}	51.1±0.74^{d}	7.4±0.21^{b}	309.2±1.47^{e}	29.3±0.57^{g}
C-H NF						
0.01	58.9±0.75^{fg}	11.8±0.77^{d}	62.3±0.71^{bc}	7.8±0.24^{b}	315.9±2.05^{d}	30.2±2.15^{f}
0.03	65.3±1.28^{e}	12.4±0.60^{c}	61.1±2.38^{bc}	8.1±0.03^{b}	312.8±1.71^{de}	33.0±1.23^{e}
0.06	69.9±2.30^{d}	11.9±0.49^{d}	61.8±2.48^{bc}	8.5±0.08^{ab}	316.8±0.74^{d}	42.1±1.13^{c}
0.09	70.9±0.63^{d}	14.4±0.61^{a}	63.9±2.40^{b}	7.8±0.37^{b}	325.7±1.01^{bc}	48.6±1.08^{ab}
0.12	73.7±1.20^{c}	13.6±0.61^{ab}	64.4±2.31^{ab}	8.4±0.21^{ab}	320.3±1.09^{cd}	32.6±1.08^{e}
0.15	91.0±1.57^{a}	14.9±0.60^{a}	73.3±1.12^{a}	9.4±0.10^{a}	343.2±3.22^{a}	52.7±1.25^{a}
0.18	85.4±1.63^{ab}	12.9±0.16^{c}	65.8±1.41^{ab}	8.1±0.14^{b}	329.8±0.52^{b}	37.9±0.76^{d}

Growth parameters were recorded at physiological maturity of tomato pot plants under shade net condition. Each value is mean of triplicates and each replicate consisted of 3 plants. Error bars represent ±SE (standard error) with the same letter statistically insignificant (p=0.05) as determined by Tukey-Kramer HSD. Water (control), BCH (bulk chitosan, 0.01% dissolved in 0.1% acetic acid) and histidine (0.01%, w/v)

Table 3

Effect of C-H NF on antioxidants and defense enzymes, ROS, chlorophyll and nitrogen content of tomato in pot plant

Treatments (%)	SOD (µmol/min/g)	POD (µmol/min/g)	CAT (mmol/min/g)	PPO (µmol/min/g)	H_2O_2 (µmol/g)	O_2^- (µmol/g)	Chlorophyll (mg/g)	Nitrogen (%)
Control (Water)	0.07±0.00^{i}	0.27±0.01^{h}	0.4±0.07^{j}	1.2±0.01^{i}	197.8±5.0a	67.0±1.01a	1.5±0.05^{i}	1.40±0.02^{h}
BCH (0.01)	0.10±0.00^{h}	0.32±0.02^{g}	1.1±0.05^{i}	1.4±0.03^{h}	190.3±8.0b	62.9±3.05b	1.9±0.07^{h}	1.70±0.04^{ef}
Histidine (0.01)	0.19±0.01^{g}	0.46±0.03^{f}	2.4±0.06^{h}	1.5±0.02^{g}	182.7±4.0c	58.7±2.04c	2.1±0.06^{g}	2.30±0.05^{a}
C-H NF								
0.01	0.22±0.01^{f}	0.63±0.01^{e}	2.6±0.05^{g}	1.6±0.03^{f}	176.8±6.0d	54.2±4.03d	2.4±0.06^{f}	1.74±0.03^{e}
0.03	0.24±0.00^{e}	0.63±0.04^{e}	2.7±0.08^{f}	1.7±0.05^{d}	171.6±2.7e	48.5±2.75e	2.4±0.09^{e}	1.84±0.02^{c}
0.06	0.28±0.00^{c}	0.66±0.02^{d}	3.2±0.09^{d}	1.6±0.03^{f}	163.9±4.0f	43.4±1.53f	2.8±0.05^{d}	2.02±0.06^{b}
0.09	0.30±0.01^{b}	0.63±0.03^{e}	3.0±0.07^{e}	2.0±0.04^{b}	162.8±7.0f	36.7±3.09g	2.9±0.09^{c}	1.74±0.04^{e}
0.12	0.26±0.01^{d}	0.85±0.02^{b}	3.3±0.09^{c}	2.1±0.03^{a}	154.9±2.4g	30.1±2.43h	3.1±0.07^{b}	1.79±0.05^{cd}
0.15	0.32±0.00^{a}	0.86±0.04^{a}	3.6±0.09^{a}	2.0±0.02^{bc}	145.3±4.0h	26.2±3.37i	3.3±0.04^{a}	1.62±0.03^{g}
0.18	0.28±0.0^{0c}	0.77±0.01^{c}	3.4±0.08^{b}	1.7±0.01^{e}	165.2±5.0f	36.1±1.64g	2.4±0.09^{f}	1.62±0.03^{g}

Effect of C-H NF on antioxidants and defense enzymes, ROS, chlorophyll and nitrogen content were measured at 3rd day of second foliar application in tomato pot plants under shade net condition. Each value is mean of triplicates and each replicate consisted of 3 plants. Error bars represent ±SE (standard error) with the same letter statistically insignificant (p=0.05) as determined by Tukey-Kramer HSD. Water (control), BCH (bulk chitosan, 0.01% dissolved in 0.1% acetic acid)

A

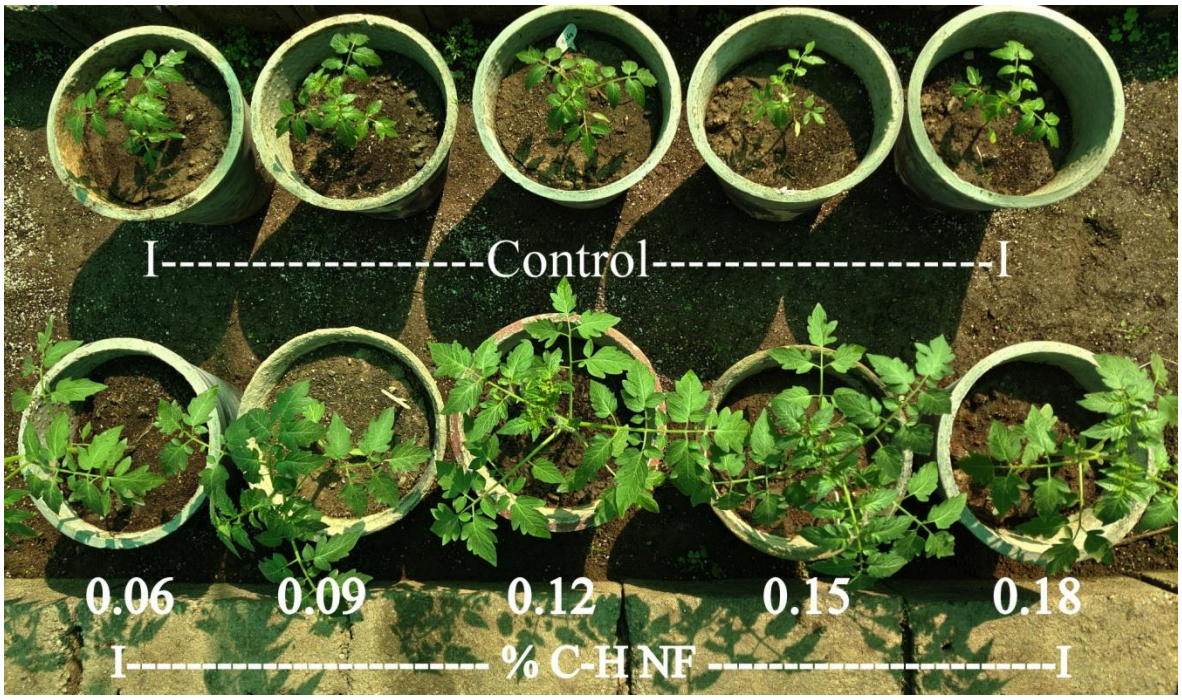

B

Figure 6. Effect of C-H NF on (A) plant growth (B) root growth of tomato in pot experiment

Discussion

The ionic gelation method is employed for the synthesis of C-H NF, wherein TPP serves as a crosslinker [20]. Through this approach, nanomaterials can be effortlessly tailored to achieve desired size ranges, PDI, and zeta-potential [2, 36]. The positively charged functional groups ($–NH_3^+$) of chitosan (0.5%) in an acidic medium interact with the negatively charged $–PO_4^-$ (phosphate) group of 0.5% TPP (ionic cross-linker), leading to the formation of crosslinked chitosan+TPP complex. The procedure is primarily characterized by ionic cross-linking. In this approach, various concentrations of histidine (0.5, 1, 1.5, 2, 2.5, and 3%; w/v) are used to interact with the chitosan+TPP complex. During the crosslinking process, some $–NH_3^+$ groups remain unbound and accessible for subsequent interaction with histidine. The functional groups of histidine (–C=O and –C-N) further interact with the chitosan+TPP complex, resulting in the formation of a condensed nanoscale C-H NF. Based on the FTIR study, an amidation reaction, occurring between amine groups (–NH) of chitosan and carboxyl group (–C=O) of histidine produced the chitosan-histidine as represented in Fig. 3A and B [13]. Among the various concentrations of histidine, 2% histidine was chosen based on the findings of the DLS study (Fig. 4). After freeze drying, approx 386 mg C-H NF dry powder was obtained from each reaction. Unlike chitosan, the synthesized nanoformulation completely dissolved in distilled water.

The optimization of the final histidine concentration for the synthesis of chitosan-histidine nanoformulation was systematically conducted, taking into account multiple parameters, including z-average (nm), PDI, zeta potential (mV), conductivity (mS/cm), kcps, and DCR, as well as encapsulation efficiency (EE). The nanoformulations synthesized at concentrations ranging from 0.5% to 1.5% exhibited z-average values for diameter, ranging from 527.1 to 396.3

nm and PDI ranging from 0.495 to 0.337 (Fig. 4A and B). Moreover, in the context of encapsulation efficiency (EE), it is crucial to assess the degree of interaction between the chitosan-TPP complex and histidine within the C-H NF. To assess the encapsulation efficiency (EE), a ninhydrin test was performed on the supernatant obtained during the purification step of synthesis to estimate the free amino acid content. The encapsulation efficiency ranged from 37% to 47%, while the yield ranged from 21.26% to 27.42% within this concentration range (0.5% to 1.5%) (Fig. 4G and H). Furthermore, in the concentration range of 0.5% to 1.5%, the formulation's viscosity and conductivity demonstrated an increase (Fig. 4D and I), attributed to the saturation of all charged functional groups associated with chitosan and histidine[13]. It was noted that an increased propensity for chitosan-TPP interactions was discerned in contrast to the chitosan-TPP-histidine complex (Fig. 5A). This is attributed to the insufficient amount of histidine available for interaction with chitosan-TPP during ionic gelation. Consequently, this deficiency led to diminished encapsulation efficiency and yield. Furthermore, within the histidine concentrations range of 2.5% to 3%, an escalation in the z-average was noted, rising significantly from 358.7 to 678.6 nm. Concurrently, the PDI value, viscosity, and conductivity also exhibited an increase (Fig. 4A, B, D and I). It is postulated that, under these conditions, a chitosan-TPP-histidine complex, along with a more intricate chitosan-TPP-histidine structure, was formed (Fig. 5C). Moreover, at these concentrations, interactions between histidine molecules (histidine-histidine) were observed due to the elevated histidine concentration (Fig. 5C). The escalation in PDI was attributed to excess histidine facilitating intermolecular interactions between histidine molecules [37]. However, the encapsulation efficiency and yield percentage of the formulation decreased at histidine concentrations surpassing 2.5% (Fig. 4G and H). This reduction is attributed to the interaction of his-his, coupled with multiphase interactions of chitosan-TPP-

299 histidine due to the surplus availability of histidine. Some studies have documented that an
300 excess of histidine in aqueous solutions leads to the formation of hydrogen bonding and
301 dipeptide bonds between histidine-histidine [37, 38]. Furthermore, the concentration range of
302 0.5-3% (Fig. 4C), illustrates a slight reduction in the zeta potential with an increase in
303 concentration. The observed phenomenon suggests that the zeta potential is responsive to
304 variations in histidine concentration, indicative of its dependence on the presence of influenced
305 by the availability of free functional groups in nanoformulations. The increased concentration of
306 histidine led to the occupancy of the $-NH_2$ group of chitosan, despite the presence of its
307 functional group in the form of the protonated $-NH_2$ group of the imidazole ring.
308 Among the various histidine concentrations investigated, a 2% concentration was employed to
309 synthesize C-H NF. The resulting C-H NF exhibited z-average of 314.4 nm, a PDI of 0.218, a
310 zeta potential of 11.2 mV, conductivity of 0.046 mS/cm, viscosity of 1.43 Cps, kilo-counts per
311 second (kcps) of 406.5, derived count rate (DCR) of 1446.4, encapsulation efficiencies of 53%,
312 and yield percentage of 32.17% (Fig. 4A-I). Lower PDI and viscosity may enhance the
313 interaction between nanoparticles and plant cells, facilitating nutrient absorption. Further, the
314 conductivity of the solution was influenced by the concentration of histidine in the solution. In
315 addition, the primary influences in diminishing the size of the chitosan particles were most
316 marked in the solution's viscosity and conductivity. Size and zeta potential are critical
317 characteristics influencing the interaction of nanomaterials with plant cells, impacting physico-
318 biochemical responses in plants [39]. Positive zeta potential in C-H NF is noteworthy, as it
319 contributes to the stability of nanoformulations in aqueous solutions and enhances their
320 interaction with negatively charged plant cell surfaces [24]. The significantly lower PDI value at
321 2% histidine concentration indicates that the nanoformulation predominantly consisted of the

chitosan-TPP-histidine complex (Fig. 5B). The positive zeta potential of the prepared nanoformulation along with the low PDI indicates its colloidal stability for use in agriculture applications. A lower PDI signifies a homogeneous distribution of particle sizes, preventing the agglomeration of smaller particles into larger ones. The uniformity in nanoparticle sizes is crucial for facilitating facile entry into plant cells through cellular passages and surface openings [40]. Furthermore, maintaining a lower PDI (0.180) not only ensures stability but also augments the overall bioactivity [41, 42]. Maintaining this reduced PDI is crucial for stability and increased bioactivity, as underscored in studies [43, 44]. The C-H NF, formulated with 2% histidine, underwent further characterization through a Nanoparticle Tracking Analysis (NTA). This investigation revealed a substantial concentration of nanoparticles, quantified at 3.53×10^8 particles per ml, with an average size of 341.6 nm at pH 7 in an aqueous environment (Fig. 2A and B). The efficacy of nanoformulations in cellular systems is contingent upon achieving a higher particle concentration per unit volume of the formulation [2]. In our research, the notable concentration per ml of C-H NF (3.53×10^8) signifies efficacy in enhancing higher biological activities.

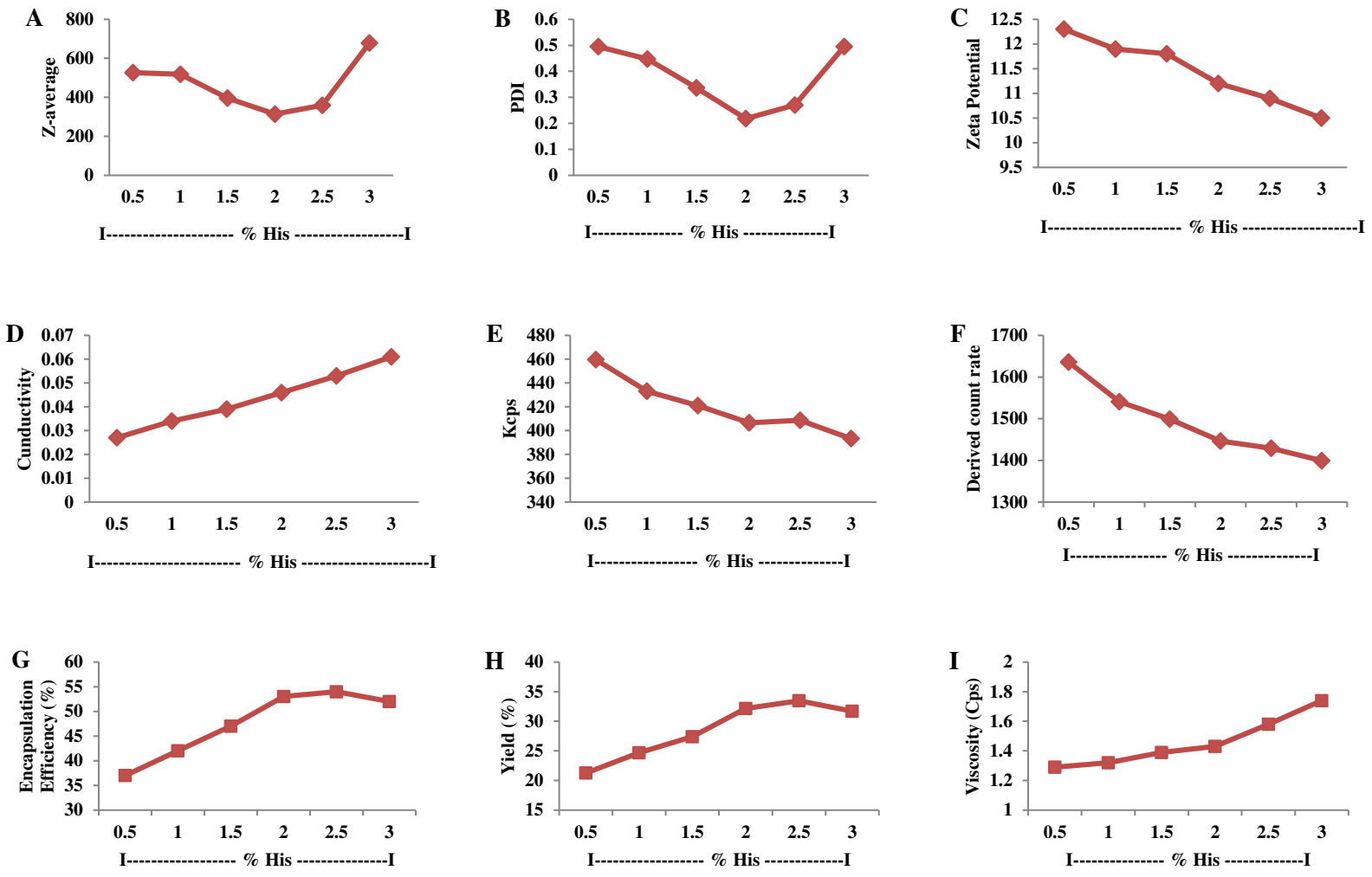

341 **Figure 4**. Effect of different concentrations of histidine (0.5-3%) on (a) z-average (b) PDI (c) zeta potential (d) conductivity (e) Kcps (f)
342 Derived count rate (g) encapsulation efficiency (%) (h) yield (%) and (i) viscosity of chitosan-histidine nanoformulation (C-H NF)

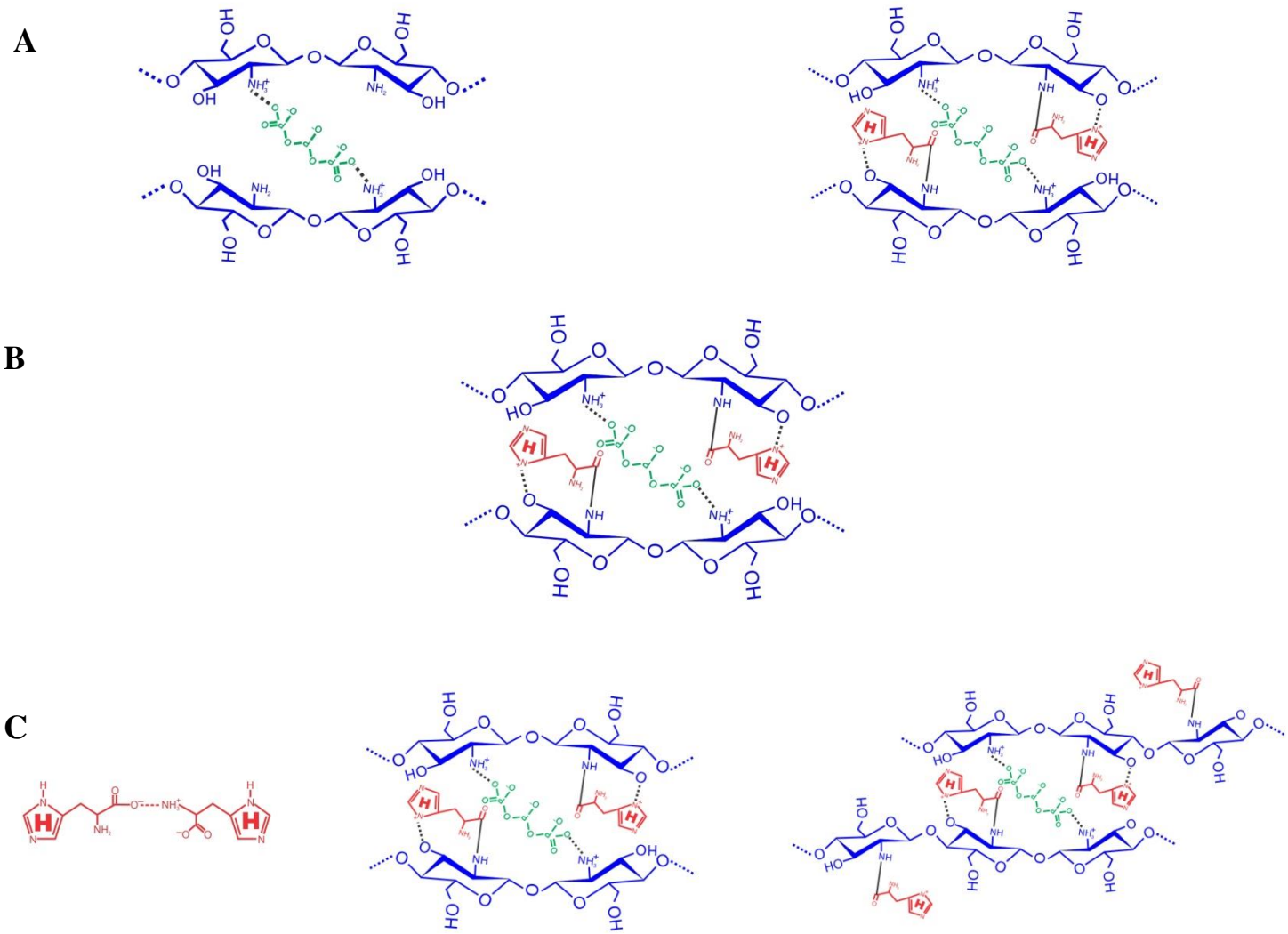

Figure 5. Hypothetical model representing interaction of CS, TPP and His.

The FTIR spectra facilitated the identification of intermolecular connections among the functional groups present in chitosan, histidine, and C-H NF (Fig. 3A and B). Specifically, the FTIR spectrum of chitosan (Fig. 3A) exhibited distinctive absorption bands at characteristic wavenumbers, including 3439 cm^{-1} (attributed to $–NH_2$ and –OH stretching), 1659 (indicative of $–CONH_2$ bending), 1568 (corresponding to $–NH_2$ bending), and 896 cm^{-1} (associated with the anhydrous glycosidic bond). The major characteristic peak at 3417 cm^{-1} observed in the FTIR spectrum of C-H NF is found to correlate with the $–NH_2$ and –OH groups inherent in the bulk chitosan present in C-H NF (Fig. 3A and B). Furthermore, a notable shift in peak position is evident, with the peaks moving to 1654 (reflecting $–CONH_2$), 1543 (indicative of $–NH_2$), and 890 cm^{-1} (associated with the anhydrous glycosidic bond) as compared to bulk chitosan. This observed shift in peak positions provides valuable insight into the interaction dynamics between chitosan and TPP, underscoring the structural alteration in the formation of C-H NF [24, 40]. The FTIR analysis of C-H NF revealed a distinctive peak at 1648 cm^{-1}, corresponding to the C=O group of histidine, indicating an interaction with the $–NH_2$ group of chitosan [13, 45]. Additionally, in chitosan, the peaks at 2879 cm^{-1} intensified in C-H NF, shifting to 2882 cm^{-1}, suggesting amidation of chitosan. Furthermore, a plausible interaction involving the imidazole ring of histidine and the –OH group of chitosan was inferred from the shift in the peak from 3439 to 3417 cm^{-1}. Based on these findings, a hypothetical structure model of C-H NF was proposed, illustrating the various interactions (Fig. 3C and D). Subsequently, SEM (EVO MA10, Carl Zeiss Promenade, Jena, Germany) and TEM (HR-TEM, JEOL, JEM 2100F, USA) studies confirmed the surface morphology and internal structure of the nanoformulations, respectively. SEM study showed a spherical-shaped nanomaterial with a porous structure (Fig. 3E). However, the TEM study revealed that it has mild pores over the structure (Fig. 3F and G). The high

porosity of the external and internal surface of nanomaterial gives a higher surface area which is responsible for more interaction with the plant surface and surface receptors [2, 45]. In previous studies, similar external and internal architecture was confirmed in chitosan and TPP-based chitosan nanoformulations [2, 36].

The current investigation focused on the impact of varying concentrations of C-H NF (0.001, 0.003, 0.006, 0.012, and 0.015%, w/v) on seedling growth with observation made after a 10-day germination period. The results indicate a noteworthy influence on tomato seedlings, with a significantly higher germination % (95.9-99.8%). Additionally, the C-H NF exhibited significant improvements in shoot length (13.6-16.2 cm), root length (10-13.9 cm), and SVI (2556.6-2895.1) in 0.006-0.015% concentrations of C-H NF over the histidine (Table 1).

In the current research, the supplementations of C-H NF resulted in a noteworthy enhancement of growth characteristics in tomato plants during a potted experimental regimen. This effect was observed to be superior compared to untreated control, bulk chitosan, and histidine (Table 2). Considering the growth promoting there was a massive difference between the C-H NF and its bulk form. The efficacy of the nanoformulation surpassed that of the bulk form, even when applied at equivalent levels. The results unveiled an augmentation in growth attributed to the application of C-H NF across all the parameters. These parameters include plant height, number of leaves per plant, number of branches per plant, leaf area, stem diameter, and root length. The growth-enhancing effect was observed across a concentration range of 0.01 to 0.18%. However, at a 0.15% concentration of the nanoformulation, maximum values were observed for all growth parameters (Table 2; Fig. 6). The activity of SOD ranges from 0.22-0.32 µmol/min/g, significantly surpassing the levels in the control (0.07µmol/min/g), BCH (0.10µmol/min/g) and histidine (0.19 µmol/min/g) across all concentration of C-H NF (Table 3). Similarly, the

activities of POD (0.63-0.86 µmol/min/g), CAT (2.6-3.6 mmol/min/g), and PPO (1.6-2.1 µmol/min/g) were higher in all concentrations of C-H NF compared to histidine, BCH and control (Table 3). Further, foliar application of chitosan nanoformulations extensively mitigated ROS levels and maintained cellular homeostasis by fostering the activities of antioxidant and defense enzymes. However, the content of H_2O_2 (176.8-145.3 µmol/g) and O_2^{-1} (54.2-26.2 µmol/g) in all concentrations of C-H NF (0.01 to 0.18%) was prominently lower as compared with control, BCH and histidine (Table 3). The higher activity of chitosan nanoformulations in treated plants effectively counteracted the level of ROS (H_2O_2 and O_2^-) in the leaves [43, 46, 47]. Previous studies have revealed the role of increased antioxidant enzyme activity in reducing ROS level in the plants [40, 44]. Our findings align with this, as we observed that higher activity of SOD, POD, CAT, and PPO significantly controlled the concentration of H_2O_2 and O_2^- in tomato pot plants. Furthermore, the total chlorophyll content (2.41-3.30 mg/g) of pot plants in all the concentrations of C-H NF (0.01 to 0.18) exhibited noteworthy enhancement compared to the control (1.56mg/g), BCH (1.94mg/g), and histidine (2.17mg/g) (Table 3). Additionally, the N content (1.62%-2.02%) was significantly higher in all concentrations of C-H NF (0.01-0.18%) compared to the control (1.40%) (Table 3). The increased levels of chlorophyll and nitrogen are important for the higher rate of photosynthesis, contributing to enhanced plant growth and yield [36].

Numerous reports have documented the development of chitosan nanoformulations employing the ionic gelation method with emphasis on the utilization of TPP [2, 24, 36, 42, 43, 48, 49]. These nanoformulations have been used to enhance plant immunity against plant diseases and growth for getting an adequate yield. However, limited literature is available where chitosan histidine nanoparticles have been developed without TPP for metal ion absorption [9-12], drug

delivery [13], gene delivery [14-16], cancer therapy [17], and wound healing [18]. To the best of current knowledge, chitosan histidine nanoformulations have not undergone evaluation for their impact on physiological and biochemical responses in plants. In the current investigation, a chitosan nanoformulation functionalized with histidine was explored, revealing notable changes in the physico-biochemical properties of C-H NF. Previous studies on chitosan nanomaterials have reported various ranges of PDI ranging from 0.3 to 0.5 [2]. In our research, the PDI was significantly lower compared to the previously reported chitosan nanomaterials, supporting its higher physiological and biochemical impact on tomato plants, likely attributed to its homogenous interaction with plant cells. Previous investigations have demonstrated elevated zeta potential in chitosan nanoformulation, attributed to the presence of freely available positively charged $–NH_2$ group in chitosan [2, 43, 48, 49]. In the current formulation (C-H NF), histidine has been incorporated, introducing its functional group with a positive charge. The addition of this functional group has not significantly changed the zeta potential, resulting in a balanced zeta potential. However, higher encapsulation efficiency and lower PDI have been observed. The concentration of nanomaterials in aqueous solutions is crucial for maximizing their effectiveness in plants. It is very important for its higher activity in plants and the determination of concentration of nanoparticles has been reported previously on chitosan nanomaterials [40]. In our study, a considerably higher nanoparticle concentration/ml was recorded through NTA analysis. The higher concentration of nanoparticle/ml is presumed to have contributed to the higher bioactivity of nanoformulation in tomato plants. Moreover, the presence of an FTIR peak at 1648 cm^{-1} in C-H NF confirmed the interaction between –C=O of histidine and $–NH_2$ group of chitosan through amide linkage [13]. Furthermore, the –CN group of histidine (Imidazole ring) may have interacted with the –OH group of chitosan, facilitated by

436 the protonation of the –NH group of the imidazole ring in an acidic medium [13, 50].
437 Furthermore, the observed biological activity in tomato plants can be attributed to two facts. The
438 physico-biochemical properties of chitosan-histidine nanoformulations, characterized by a lower
439 z-average and PDI value, along with a positive zeta potential, are considered influential.
440 Furthermore, higher conductivity, kcps, DCR, and nanoparticle concentration/ml contribute to
441 enhanced growth and development. Moreover, the potential biological activity of histidine in the
442 plants cannot be discounted, as its presence entails three N atoms that may serve as an N source
443 of the plant and function as an organic N source. Previous studies have suggested the role of
444 histidine in plant metabolism as both a structural and functional component [7, 8].

445 The current research asserts that the anticipated positive impact of C-H NF on tomato crops can
446 be attributed to its inherent physicochemical properties, including homogenous-sized
447 nanoparticles, lower PDI, higher zeta potential, and higher nanoparticle concentration/ml. More
448 specifically, the biochemical and physiological responses of tomatoes to C-H NF may occur
449 through a synergic effect involving histidine and chitosan. To elaborate further, C-H NF
450 contained a total of four nitrogen, three from histidine and one from chitosan. Consequently, the
451 nanoformulation could act as a potential organic nitrogen source for tomatoes, potentially
452 contributing to enhanced growth. Notably, at a dosage of 0.009%, C-H NF prompted positive
453 effects on seedling growth in the Petri plate. Moreover, in potted plants, the foliar spray of C-H
454 NF (0.15%) proved effective across all growth parameters. It maintained antioxidant-defense
455 enzyme activities, balanced ROS content, and considerably enhanced chlorophyll and nitrogen
456 content. According to the findings, the current study claims that the application of C-H NF can
457 be implemented in field experiments for translation and validation of technology.

458 **Materials and methods**

Materials

Chitosan of low molecular weight (50,000–190,000 Da, 80% degree of deacetylation), sodium tripolyphosphate (TPP), and histidine were procured from Sigma-Aldrich, St. Louis, MO, USA. Other chemicals were sourced from HiMedia and SRL, Mumbai, India. Deionized (DI) water was used in the study. Seeds of tomato cultivar 'NBH-2453' were used from Nobel Seeds Pvt. Ltd., India.

Synthesis of chitosan-histidine nanoformulations

To synthesize C-H NF, the ionic gelation method was explored[19,20]. In this method, 0.5 % chitosan was dissolved in glacial acetic acid (1% v/v) to get a pH of 3.84. NaOH solution was then used to adjust the processed chitosan (0.5%) to pH 5.10 followed by cross-linking with 0.5% TPP. The cross-linking was conducted using a pediatric set (Romsons, Agra, India) under a magnetic stirrer (200 rpm; Remi Laboratory Instruments, Mumbai, India). Before completing the cross-linking, the chitosan-TPP complex further interacted with different concentrations of histidine solutions (0.5, 1, 1.5, 2, 2.5, and 3%; w/v). The final concentration of histidine was optimized based on the DLS study. The formulation was further centrifuged (10,000 rpm for 10 min), and precipitated semisolid material was resuspended in DI water and sonicated (Q 500 Sonicator Qsonica, USA) for 4 min with 5-second pulse on/off, 40% amplitude. This process was repeated three times. The obtained semi-solid formulation was lyophilized (FreeZone 6, Labconco, USA), and stored at room temperature.

Characterization of chitosan-histidine nanoformulations

Chitosan-histidine nanoformulations underwent comprehensive characterization utilizing dynamic light scattering (DLS) on a Zetasizer instrument (ZS90, Malvern, U.K.). Measurements were conducted at 25°C, employing a scattering angle of 90°C. Key parameters including Z-

averages, size distribution, PDI, zeta potential, conductivity, kcps, and DCR were determined through triplicate measurements, ensuring robust and reliable data acquisition. Various concentrations of histidine solutions, ranging from 0.5% to 3% (w/v), were used for investigation. The optimization of the final histidine concentration was selected based on a thorough analysis using DLS studies. Additionally, mean size and particle concentration (number of particles/ml) were validated through NTA (Nano Sight NS300, Malvern Panalytical, UK). The interaction among functional groups in C-H NF was assessed via Fourier transform infrared spectroscopy (FTIR; Alpha, Bruker, Germany). Lyophilized nanoformulations with potassium bromide (KBr) were triturated (in 1:99 ratios) and spectra were collected in transmittance mode at 25ºC in the 3800-600 cm^{-1} region. SEM (scanning electron microscopy), and TEM (transmission electron microscope) analyses were conducted to examine the surface morphology and internal structure. For SEM (EVO MA10, Carl Zeiss Promenade, Jena, Germany), samples were dried using critical point drying (CPD, Emitech K850) and coated with gold-palladium via a sputter coating[21]. For TEM (HR-TEM, JEOL, JEM 2100F, USA), nanoformulations were diluted with deionized water, sonicated (2 cycles) with a probe sonicator, negatively stained with 2% phosphotungstic acid (PTA) and dried at room temperature (25±2ºC) before observation[22].

EE, yield, and viscosity of C-H NF

The EE of histidine in the nanoformulations was assessed using the ninhydrin test via the spectrophotometer method[23,24]. The yield of C-H NF was calculated based on the various concentrations of histidine (0.5, 1, 1.5, 2, 2.5, and 3%) used during the synthesis of the nanoformulation. EE was calculated by following equation[24].

$$\mathrm{EE} = \frac{\text{Free amount of histidine in suparnatant}}{\text{Total amount of histidine}} \times 100$$

The viscosity was described by the Ostwald viscometer method[25]. Viscosities were calculated using the formula:

$$\frac{\eta_s}{\eta_w} = \frac{\rho_s}{\rho_w}\frac{t_s}{t_w}$$

***In-vitro* seedling growth**

The seedling growth of Tomato variety 'NBH 2453' was investigated in a Petri plate using standard methods with minor adjustments[26]. Briefly, the seeds underwent a 1-hour treatment with various concentrations of C-H NF (0.001, 0.003, 0.006, 0.009, 0.012, 0.015, and 0.018% w/v), in addition to control (water), bulk-chitosan (0.01%; w/v) and histidine (0.01%; w/v) all dissolved in DI water. In this experiment, 15 days post-sowing, parameters such as seed germination percentage, shoot-root length, and seedling vigour index (SVI) were assessed. The seedling vigour index (SVI) was calculated using the formula described[27].

Seedling vigour index (SVI) = Germination % × (root length + shoot length)

Plant growth, antioxidants and defense enzymes, ROS, and chlorophyll content

Different concentrations of C-H NF were assessed through foliar spray in a pot experiment conducted under net house conditions. Tomato seeds were sown in earthen pots filled with standard potting soil sourced from the field. The synthesized nanoformulation (0.01, 0.03, 0.06, 0.09, 0.12, 0.15, and 0.18% w/v), bulk chitosan (0.01%), histidine (0.01%), and control (water) underwent two foliar applications: the first 10 days after transplanting and the second just before flowering stage. Plant growth parameters *viz*. plant height, number of leaves per plant, number of branches per plant, leaf area, stem diameter, and root length were recorded at the time of physiological maturity. Antioxidant and defense enzymes like superoxide dismutase (SOD) (EC 1.15.1.1), peroxidase (POD) (EC 1.11.1.7), catalase (CAT) (EC 1.11.1.6) and polyphenol

peroxidase (PPO) (EC 1.10.3.1) were estimated 3 days after 2nd foliar application of various treatments[28-30]. The H_2O_2 and O_2^{-}[31,32], chlorophyll[33], and nitrogen content[34] were measured after 3 days of 2nd foliar application.

Statistical analysis

Statistical analyses were performed with JMP software version 12 employing the Kramer HSD test at a significance level of $p = 0.05$[35]. All experiments were executed in triplicate, with each replication comprising a minimum of ten samples (for seedling experiments) and three samples (for pot experiments) selected randomly from the plant population.

Resources

The study was in accordance with relevant institutional, national, and international guidelines and legislation.

Acknowledgements

The work was consummated at Nano Research Facility Lab, Department of Molecular Biology and Biotechnology, MPUAT, Udaipur and RARI, Durgapura (SKNAU, Jobner), Jaipur, Rajasthan, India.

Author contributions

M.M., V.S. and A.P. designed the study. M.M., P.C. and M. conducted the laboratory experiments, synthesized and characterized nanoformulations. D.P., K.M. M.K.S, M.B.M, D.K.B. and R.S. evaluated biochemical responses and prepared figures and tables. K.K.M., B.S., S.P., N.K.G., O.P.G., Y.K.S., U.S., R.B., B.L.J. and V.S. provided overall supervision to the project. V.S., M.M. and R.S. wrote the manuscript, all authors read and revised the manuscript, and all authors approved the final version of manuscript for submission.

Data availability

All relevant data generated or analysed are included in the manuscript and the supporting materials.

Conflict of interest statement

Authors declare that they do not have any financial conflict of interest.

References

1. Ingle PU, Shende SS, Shingote PR. *et al.* Chitosan nanoparticles (ChNPs): A versatile growth promoter in modern agricultural production. *Heliyon.* 2022;**8**:e11893 doi.org/10.1016/j.heliyon.2022.e11893
2. Prajapati D, Pal A, Dimkpa C. *et al.* Chitosan nanomaterials: A prelim of next-generation fertilizers; existing and future prospects. *Carbohydr. Polym.* 2022;**288**:119356 doi.org/10.1016/j.carbpol.2022.119356
3. Adhikari HS, Garai A, Yadav PN. *et al.* Synthesis, characterization, and anticancer activity of chitosan functionalized isatin based thiosemicarbazones, and their copper (II) complexes. *Carbohydr. Res.* 2023;**526**:108796 doi.org/10.1016/j.carres.2023.108796
4. Raza ZA, Khalil S, Ayub A. *et al.* Recent developments in chitosan encapsulation of various active ingredients for multifunctional applications. *Carbohydr. Res.* 2020;**492**:108004 doi.org/10.1016/j.carres.2020.108004
5. Chen Y, Liu Y, Dong Q. *et al.* Application of functionalized chitosan in food: A review. *Int. J. Biol. Macromol.* 2023;**235**:123716 doi.org/10.1016/j.ijbiomac.2023.123716
6. Torkaman S, Rahmani H, Ashori A. *et al.* Modification of chitosan using amino acids for wound healing purposes: A review. *Carbohydr. Polym.* 2021;**258**:117675 doi.org/10.1016/j.carbpol.2021.117675
7. Krishna Deepak RNV, Sankararamakrishnan R. N–H···N hydrogen bonds involving histidine imidazole nitrogen atoms: A new structural role for histidine residues in proteins. *Biochem.* 2016;**55**:3774-3783 DOI: 10.1021/acs.biochem.6b00253.
8. Wang Y, Li P, Chen F. *et al.* A novel pH-sensitive carrier for the delivery of antitumor drugs: Histidine-modified auricularia auricular polysaccharide nano-micelles. *Sci. Rep.* 2017;**7**:4751-4760 doi.org/10.1038/s41598-017-04428-8

9. Mahl CR, Taketa TB, Rocha-Neto JBM. *et al*. Copper ion uptake by chitosan in the presence of amyloid-β and histidine. *Appl. Biochem. Biotechnol.* 2020;**190**: 949-965 doi.org/10.1007/s12010-019-03120-z
10. Taketa TB, Mahl CR, Calais GB. *et al.* Amino acid-functionalized chitosan beads for in vitro copper ions uptake in the presence of histidine. *Int. J. Biol. Macromol.* 2021;**188**:421-431 doi.org/10.1016/j.ijbiomac.2021.08.017
11. Maia MT, Sena DN, Calais GB. *et al.* Effects of histidine modification of chitosan microparticles on metal ion adsorption. *React. Funct. Polym.* 2020;**154**: 104694 doi.org/10.1016/j.reactfunctpolym.2020.104694
12. Nguyen ML, Juang RS. *et al*. Modification of crosslinked chitosan beads with histidine and Saccharomyces cerevisiae for enhanced Ni (II) biosorption. *J. Taiwan Inst. Chem. Eng*. 2015;**56**:96-102 doi.org/10.1016/j.jtice.2015.03.033
13. George D, Maheswari PU, Begum KMS. *et al.* Chitosan-cellulose hydrogel conjugated with L-histidine and zinc oxide nanoparticles for sustained drug delivery: Kinetics and in-vitro biological studies. *Carbohydr. Polym.* 2020;**236**:116101 doi.org/10.1016/j.carbpol.2020.116101
14. Akbari V, Rezazadeh M, Hanaie NS. *et al.* Preparation and in vitro characterization of histidinetrimethyl chitosan conjugated nanocomplex incorporated into injectable thermosensitive hydrogels for localized gene delivery. *Appl. Biochem. Biotechnol.* 2021;**69**:1047-1057 DOI: 10.1002/bab.2175
15. Chang KL, Higuchi Y, Kawakami S. *et al.* Development of lysine–histidine dendron modified chitosan for improving transfection efficiency in HEK293 cells. *JCR.* 2011;**156**:195-202 doi.org/10.1016/j.jconrel.2011.07.021
16. Morris VB, Sharma CP. *et al.* Folate mediated histidine derivative of quaternised chitosan as a gene delivery vector. *Int. J. Pharm.* 2010;**389**: 176-185 doi.org/10.1016/j.ijpharm.2010.01.037
17. Sun P, Huang W, Kang L. *et al.* siRNA-loaded poly (histidine-arginine) 6-modified chitosan nanoparticle with enhanced cell-penetrating and endosomal escape capacities for suppressing breast tumor metastasis. *Int. J. Nanomedicine.* 2017;**12**:3221 doi: 10.2147/IJN.S129436

606 18. Lin Z, Li R, Liu Y. *et al.* Histatin1-modified thiolated chitosan hydrogels enhance wound
607 healing by accelerating cell adhesion, migration and angiogenesis. *Carbohydr. Polym.*
608 2019;**230**:115710 doi.org/10.1016/j.carbpol.2019.115710
609 19. Saharan V, Mehrotra A, Khatik R. *et al.* Synthesis of chitosan based nanoparticles and
610 their in vitro evaluation against phytopathogenic fungi. *Int. J. Biol. Macromol.*
611 2013;**62**:677-683 DOI: 10.1016/j.ijbiomac.2013.10.012
612 20. Saharan V, Sharma G, Yadav M. *et al.* Synthesis and in vitro antifungal efficacy of Cu–
613 chitosan nanoparticles against pathogenic fungi of tomato. *Int. J. Biol. Macromol.*
614 2015;**75**:346-353 doi.org/10.1016/j.ijbiomac.2015.01.027
615 21. Rejinold SN, Muthunarayanan M, Muthuchelian K. *et al.* Saponin Loaded chitosan
616 nanoparticles and their cytotoxicity to cancer cell lines *in vitro*. *Carbohydr. Polym.*
617 2011;**84**:407-416 doi.org/10.1016/j.carbpol.2010.11.056
618 22. Zhang HK, Yao Z, Morin G. *et al.* TEM characterization of in-reactor neutron irradiated
619 CANDU spacer material Inconel X-750. *J. Nucl. Mater.* 2014;**451**:88-96
620 doi.org/10.1016/j.jnucmat.2014.03.043
621 23. Lee Y, Choi JK, Lee KJ. *et al.* Large-scale synthesis of copper nanoparticles by
622 chemically controlled reduction for applications of inkjet-printed electronics.
623 *Nanotechnol.* 2008;**19**:415604 **DOI** 10.1088/0957-4484/19/41/415604
624 24. Kumaraswamy RV, Kumari S, Choudhary RC. *et al*. Salicylic acid functionalized
625 chitosan nanoparticle: a sustainable biostimulant for plant. *Int. J. Biol. Macromol.*
626 2019;**123**:59-69 doi.org/10.1016/j.ijbiomac.2018.10.202
627 25. Saxena I, Kumar V. Automatic version of Ostwald viscometer for conductive liquids.
628 *Instrum. Exp. Tech.* 2021;**64**:327-330 doi.org/10.1134/S0020441221010322
629 26. International Seed Testing Association. International rules for seed testing. *SST.*
630 1976;**4**:51-77
631 27. Abdul-Baki AA, Anderson JD. Vigor determination in soybean seed by multiple criteria
632 1. *Crop sci.* 1973**;13**:630-633 doi.org/10.2135/cropsci1973.0011183X001300060013x
633 28. Chance B, Maehly AC. Assay of Catalase and Peroxidase. *Meth. Enzymol.* 1955; **2**:764-
634 775 doi.org/10.1016/S0076-6879(55)02300-8

29. Taneja SR, Sachar RC. Stimulation of polyphenol oxidase (monophenolase) activity in wheat endosperm by gibberellic acid, cycloheximide and actinomycin D. *Planta* 1974;**116**:133-142 doi.org/10.1007/BF00380648
30. Moerschbacher BM, Noll UM, Flott BE. *et al.* Lignin biosynthetic enzymes in stem rust infected, resistant and susceptible near-isogenic wheat lines. *Physiol. Mol. Plant Pathol.* 1988;**33**:33-46 doi.org/10.1016/0885-5765(88)90041-0
31. Elstner EF, Heupel A. Inhibition of nitrite formation from hydroxylammoniumchloride: a simple assay for superoxide dismutase. *Anal. Biochem.* 1976;**70**:616-620 doi.org/10.1016/0003-2697(76)90488-7
32. Sinha AK. Colorimetric assay of catalase. *Anal. Biochchem.* 1972;**47**:389-394 doi.org/10.1016/0003-2697(72)90132-7
33. Stangarlin JR, Pascholati SF. Activities of ribulose-1, 5-bisphosphate carboxylase-oxygenase (rubisco), chlorophyllase, β-1, 3 glucanase and chitinase and chlorophyll content in bean cultivars (Phaseolus vulgaris) infected with Uromyces appendiculatus. *Summa Phytopathol.* 2010;**26**:34-42
34. Yoshida S, Forno DA, Cock JH. *et al.* Laboratory Manual for Physiological Studies of Rice, 3rd Edition, *International Rice Research Institute, Manila.* 1976
35. SAS, JMP: User's Guide , Version 14.2. SAS Institute, Inc., Cary, NC, USA. 2019
36. Kumaraswamy RV, Kumari S, Choudhary RC. *et al.* Engineered chitosan-based nanomaterials: Bioactivities, mechanisms and perspectives in plant protection and growth. *Int. J. Biol. Macromol.* 2018;**113**:494-506 doi.org/10.1016/j.ijbiomac.2018.02.130
37. Ye MP, Li H, Zhang QL. *et al*. Intermolecular hydrogen bonds formed between amino acid molecules in aqueous solution investigated by temperature-jump nanosecond time-resolved transient mid-IR spectroscopy. *Chinese J. Chem. Phys.* 2007;**20**: 461 **DOI** 10.1088/1674-0068/20/04/461-467
38. Heyda J, Mason PE, Jungwirth P. *et al.* Attractive interactions between side chains of histidine-histidine and histidine-arginine-based cationic dipeptides in water. *J. Phys. Chem. B.* 2010:**11**:8744-8749 doi.org/10.1021/jp101031v
39. Asgari-Targhi G, Iranbakhsh A, Ardebili ZO. *et al.* Potential benefits and phytotoxicity of bulk and nano-chitosan on the growth, morphogenesis, physiology, and

micropropagation of Capsicum annuum. *Plant Physiol. Biochem.* 2018;**127**: 393-402 doi.org/10.1016/j.plaphy.2018.04.013

40. Kumar A, Prajapati D, Devi KA. *et al.* Slow-release Zn application through Zn-chitosan nanoparticles in wheat to intensify source activity and sink strength. *Plant Physiol. Biochem.* 2021;**168**:272-280 doi.org/10.1016/j.plaphy.2021.10.013
41. Kumari S, Kumaraswamy RV, Choudhary RC. *et al.* Thymol nanoemulsion exhibits potential antibacterial activity against bacterial pustule disease and growth promotory effect on soybean. *Sci. Rep.* 2018;**8**: 6650 doi.org/10.1038/s41598-018-24871-5
42. Meena M, Pilania S, Pal A. *et al.* Cu-chitosan nano-net improves keeping quality of tomato by modulating physio-biochemical responses. *Sci. Rep.* 2020;**10**:1-11 doi.org/10.1038/s41598-020-78924-9
43. Sharma G, Kumar A, Khaidem AD. *et al.* Chitosan nanofertilizer to foster source activity in maize. *Int. J. Biol. Macromol.* 2020;**145**:226-234 doi.org/10.1016/j.ijbiomac.2019.12.155
44. Kadam PM, Prajapati D, Kumaraswamy RV. *et al.* Physio-biochemical responses of wheat plant towards salicylic acid-chitosan nanoparticles. *Plant Physiol. Biochem.* 2021**;162**:699-705 doi.org/10.1016/j.plaphy.2021.03.021
45. Kim UJ, Lee YR, Kang TH. *et al.* Protein adsorption of dialdehyde cellulose-crosslinked chitosan with high amino group contents. *Carbohydr. Polym.* 2017;**163**:34-42 doi.org/10.1016/j.carbpol.2017.01.052
46. Das K, Roychoudhury A. Reactive oxygen species (ROS) and response of antioxidants as ROS-scavengers during environmental stress in plants. *Front. Environ. Sci.* 2014;**2**:53 doi.org/10.3389/fenvs.2014.00053
47. Signorelli S, Coitino EL, Borsani O. *et al.* Olecular mechanisms for the reaction between OH radicals and proline: insights on the role as reactive oxygen species scavenger in plant stress. *J. Phys. Chem. B.* 2014;**118**:37-47 doi.org/10.1021/jp407773u
48. Kumaraswamy RV, Saharan V. Kumari S. *et al.* Chitosan-silicon nanofertilizer to enhance plant growth and yield in maize (*Zea mays L.*). *Plant Physiol. Biochem.* 2021;**159**:53-66 doi.org/10.1016/j.plaphy.2020.11.054
49. Choudhary RC, Kumari S, Kumaraswamy RV. *et al.* Characterization methods for chitosan-based nanomaterials. *Advances in the Understanding of Nanomaterials*

Research and Applications (pp. 103-116). Plant Nanobionics 2019 doi.org/10.1007/978-3-030-12496-0_5

50. Miyagi M, Nakazawa T. Determination of p K a values of individual histidine residues in proteins using mass spectrometry. *Anal. Chem.* 2008;**80**:6481-6487 doi.org/10.1021/ac8009643

TABLES' & FIGURES' CAPTIONS

Table 1. Effects of C-H NF on tomato seedling growth in *in-vitro*

Table 2. Effect of C-H NF on growth parameters of tomato in pot plant

Table 3. Effect of C-H NF on antioxidants and defense enzymes, ROS, chlorophyll and nitrogen content of tomato in pot plant

Figure 1. DLS analysis of C-H NF for (a) size (b) zeta-potential and (c) size distribution by number

Figure 2. NTA analysis of C-H NF (a) size (b) concentration of particle/ml

Figure 3. FTIR spectra of (A) bulk chitsan (B) C-H NF (C), (D) hypothetical model of C-H NF showing interactions of chitosan, TPP and histidine and SEM and TEM study of C-H NF, SEM at (E) 20kx, TEM at (F) 60kx (G)150kx

Figure 4. Effect of different concentrations of histidine (0.5-3%) on (a) z-average (b) PDI (c) zeta potential (d) conductivity (e) Kcps (f) Derived count rate (g) encapsulation efficiency (%) (h) yield (%) and (i) viscosity of chitosan-histidine nanoformulation (C-H NF)

Figure 5. Hypothetical model representing interaction of CS, TPP and His

Figure 6. Effect of C-H NF on (a) plant growth (b) root growth of tomato in pot experiment